GeoArabia, Vol. 8, No. 3, 2003
Gulf PetroLink, Bahrain

Lateral clay injection into normal faults

Wouter van der Zee, Janos L. Urai and Pascal D. Richard

ABSTRACT

The clay content of fault gouge is one of the main factors controlling transport and mechanical properties of a fault zone. This paper addresses the process of lateral clay injection into normal faults, which is one of the many processes contributing to the development of clay smear, and can lead to local enrichment of clay in a fault gouge. We combined field observations with geomechanical models to quantify the parameters leading to lateral clay inje ction into fault zones. Detailed field study shows that a releasing fault bend in a clay layer is required for clay injection to occur. The clay injection process is often associated with the formation of a branch in the fault and the development of a "squeezing block" which injects the clay into the fault zone. A simple analytical model predicts the onset of clay injection when $C = \sigma'_v (1 - \sin \phi) / (2 \cos \phi)$, where C is cohesion (MPa), σ'_v is vertical stress (MPa) and ϕ (°) is friction angle. More detailed analysis using 2-D geomechanical finite element models is in good agreement with the analytical models and allows study of the system at higher fault throw. Results of sandbox models containing layers of an elastoplastic clay analogue also compare well with field observations and numerical models, and show the initiation of the releasing step and the evolution of the clay injection process with increasing fault throw. Using our results it is possible to predict the likelihood of lateral clay injection in the subsurface, in settings like the Gharif formation of the Haushi group of Central and South Oman or the Natih formation of North Oman. This requires an estimation of the mechanical properties of the clays at the time of faulting; data which can be obtained from wireline logs and cuttings. This approach to fault seal analysis emphasizes the mechanical aspects of the clay smear process, in addition to the kinematics which were considered in previous analyses. Its application should lead to improved prediction of fault seal processes in the subsurface.

INTRODUCTION

Many hydrocarbon accumulations are affected in some way by the presence of faults in the reservoir and / or seal lithologies. In exploration and appraisal workflow, evaluation of the different leak pathways from a structure (Figure 1a) usually involves an assessment of the transport properties of faults. The two end-member cases here are flow along the fault (fault is completely open) and no flow in any direction (fault is completely sealing). The case in-between where there may be a seal along the fault but flow across the fault, or even more complicated systems of limited sealing over shorter distances in either direction, are the most complex. This is illustrated in Figure 1, which attempts to generalize systems containing layers of strongly contrasting lithologies, such as sand-clay sequences (e.g. in most Tertiary deltas, van der Zee, 2002) or carbonate-clay sequences (e.g. the Natih formation of North Oman, van Buchem et al., 2002). If the fault shown in Figure 1a is sealing in both directions, the maximum hydrocarbon column is controlled by the spill point. On the other hand, if leakage along the fault is possible, only a very small accumulation will form, controlled by the four-way dip closure in the top of the structure. Finally, across-fault leakage results in an accumulation controlled by the across-fault leak point. On the timescales of hydrocarbon production, the relative importance of sealing and non-sealing faults is quite different, and faults which have not played a role in the accumulation of oil or gas in a structure may form important flow barriers.

The first step in evaluating possible across-fault flow pathways consists of an analysis of possible juxtapositions across the fault. Although the principle can be illustrated in profile (Figure 1b, c) the analysis is necessarily a 3-D process, considering the topology of the fault system (Figure 2a) and the variation in offset along the fault (Figure 2b). The final analysis is usually carried out using a fault plane diagram constructed in a plane parallel to the fault plane (Figure 2c).

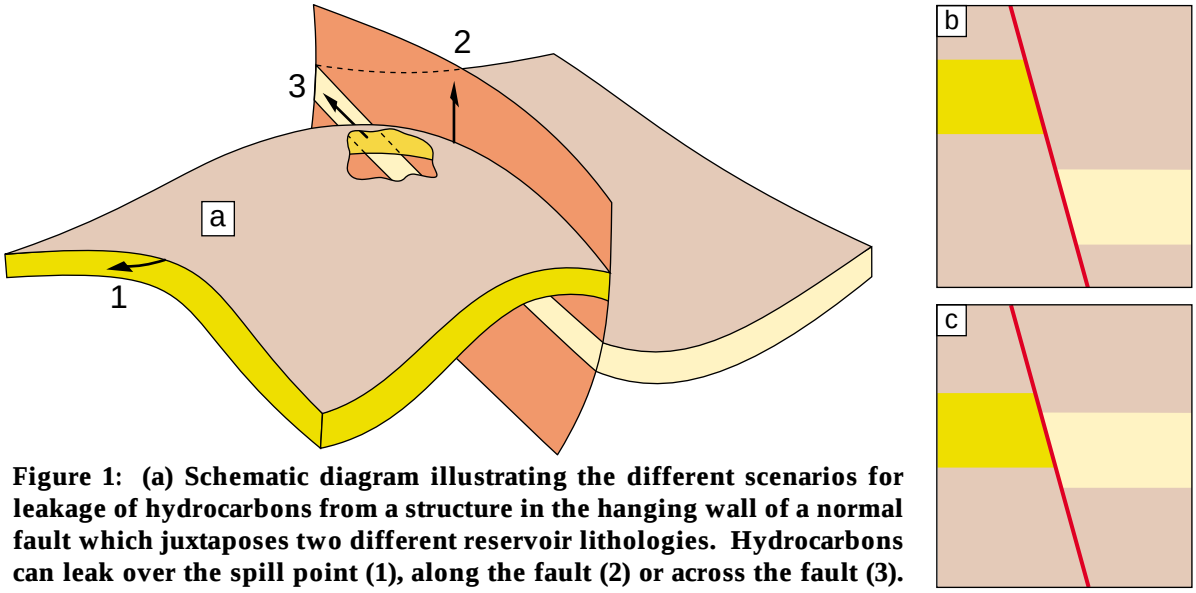

Figure 1: (a) Schematic diagram illustrating the different scenarios for leakage of hydrocarbons from a structure in the hanging wall of a normal fault which juxtaposes two different reservoir lithologies. Hydrocarbons can leak over the spill point (1), along the fault (2) or across the fault (3). The extent of mechanisms (2) and (3) is determined by the transport properties of the fault zone. (b) Lateral seal of a reservoir by juxtaposition against a low-permeable lithology. In this case, fluid flow along the fault is the only possible leak mechanism. (c) Juxtaposition of two permeable lithologies may be associated with fluid flow along the fault, across the fault or sealing in both directions by an impermeable fault gouge.

An example of such an analysis is presented by Richard et. al. (1998), for the sandstone-shale sequence of the Gharif formation of Central Oman.

In the case of juxtaposition of permeable lithologies (Knipe et al., 1997), the transport properties of the fault gouge are the critical parameter controlling fluid flow. Especially in layered sequences where one of the lithologies is much less permeable than the other, for example the Natih formation of North Oman (van Buchem et al., 1996, 2002), the redistribution and connectivity of the impermeable lithology is of interest.

Prediction of the internal structure of fault gouges is difficult, due to the large amount of highly complex processes involved. The initially segmented geometry of fault zones and subsequent coalescence of segments, in combination with the contrast in mechanical and transport properties between the layers are the two most important factors in this evolution. The resulting range of structures are illustrated in Figures 3 and 4.

It is clear from the above that fault zones can have vastly higher or lower permeability than their country rocks, and thus form either barriers or conduits for fluid flow. The amount and type of clay in a fault is one of the main parameters controlling the mechanical strength and fluid transport properties of the fault gouge (Logan and Rauenzahn, 1987; Lupini et al., 1981; Heynekamp et al., 1999; and Rawling et al., 2001). Examples are sand-shale sequences in Tertiary deltas (Weber et al., 1978) or the Gharif formation of Northern Oman (Richard et al., 1998). Much of the current research on fault seal is therefore focused on the process of clay being incorporated into the fault gouge, often called “clay smear”.

Clay smear is a loosely defined term born in hydrocarbon geology (van der Zee, 2002; Aydin and Eyal, 2002; Yielding, 2002); its usage differs between publications, and the definition of processes operating is often unclear. In the most general meaning, the term includes all processes, which somehow transform clay in the wall rock into clay that is part of the fault zone. Processes included are clay abrasion (Lindsay et al., 1993), shear in releasing fault links (Bahir Koledoye et al., 2000), preferred smear and lateral clay injection (Lehner and Pilaar, 1997; van der Zee and Urai, 2001).

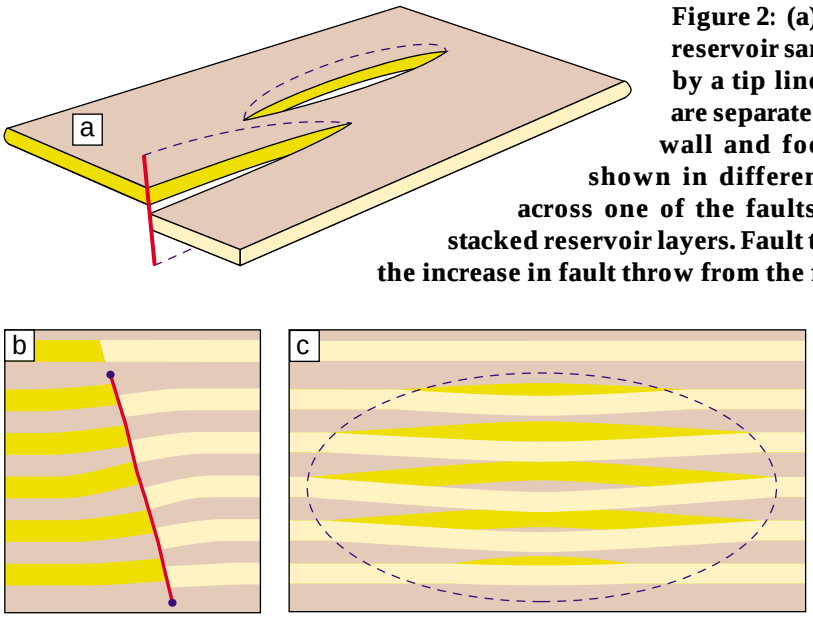

Figure 2: (a) Schematic diagram showing a reservoir sand containing two faults bound by a tip line (dashed line). The two faults are separated by a relay ramp. The hanging wall and footwall parts of the layers are shown in different shades. (b) Vertical profile across one of the faults in (a), now showing several stacked reservoir layers. Fault tip is shown by blue dots. Note the increase in fault throw from the fault tip to the center. (c) Fault plane diagram drawn in a plane parallel to the fault plane, showing juxtaposition of footwall and hanging wall units. Tip line of the fault is shown by dashed line. In the case of across-fault flow several of the layers are brought into communication by the presence of the fault.

For applied studies of clay smear evaluation a number of semi-empirical tools are available (Bouvier et al., 1989; Fulljames et al., 1997; Lindsay et al., 1993; Fristad et al., 1997). An overview and comparison of these methods is given by Yielding et al. (1997) and Yielding (2002). Most of these methods are based on the assumption that the fault gouge is a reworked equivalent of the wall rock without addition or removal of material, and therefore has, on average, the same clay fraction. Although in settings without major clay injection SGR does correlate to the amount of clay in the fault (van der Zee, 2002; Yielding, 2002), unfortunately these methods are statistical in nature, and do not specify which of the different structures shown in Figure 3 is present. Therefore predictions based on this method have a high degree of uncertainty. Other authors proposed that clay smear can produce more clay in the fault than expected from the mudstone-sand ratio in the wall rock (Lehner and Pilaar, 1997; Fulljames et al., 1997). These models assume that a releasing bend in the fault is formed in the clay layer (Figure 5), and that during fault movement the clay flows from a source layer into the pull apart structure.

In this paper, we focus on one of the processes shown in Figure 3, the lateral injection of clay into normal faults (Figure 3e). We present the results of an integrated study of the process of lateral clay injection into normal faults. Detailed field observations on well-defined fault systems in excellent outcrops are the basis for identification of the kinematics of the process. These are subsequently quantified in a series of geomechanical finite element models. Because finite element modeling is not well suited to simulate the large strains in an evolving fault gouge, results of analogue modeling with sand and clay analogues are compared with these models. Finally we discuss the application of our results to predict the clay content in fault zones in the subsurface.

FIELD OBSERVATIONS

Study Area

We studied two outcrops with excellent exposure and a well known geology. Details of the observations are published elsewhere (van der Zee, 2002).

In this paper we focus only on the structures associated with lateral clay injection.

Airport Road Outcrop, Miri, Malaysia

The first example comes from the airport road outcrop near Miri, Malaysia. This outcrop in Miocene deltaic sediments is described in detail by Burhannudinnur and Morley (1997), Lesslar and Wannier

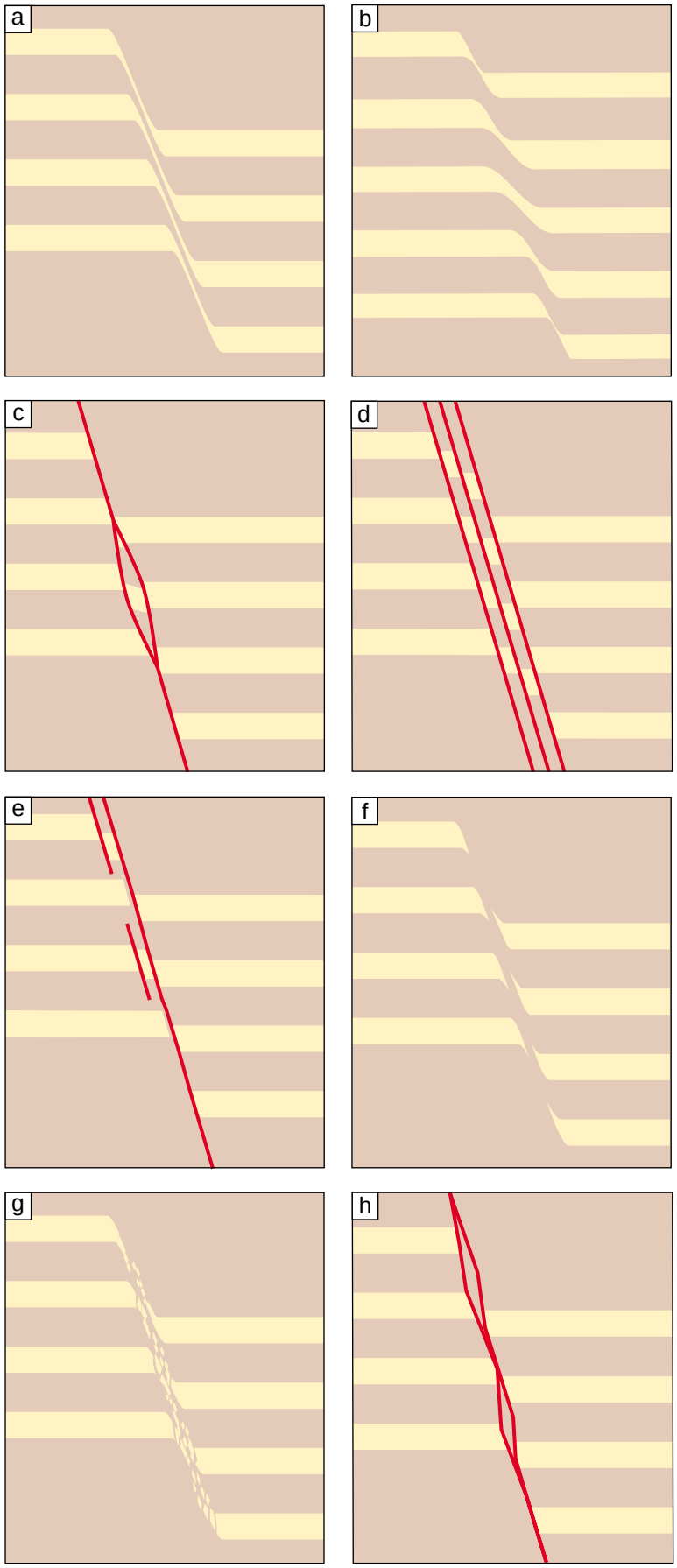

Figure 3: An illustration of the main structural elements found in fault zones in sediments. After van der Zee and Urai (2001). (sand = yellow; clay = grey)

(a) Heterogeneous simple shear deformation, without strong localization in a discrete fault plane.

(b) Heterogeneous simple shear, with lateral transition into a sharply localized zone of deformation.

(c) Lens structure between two branches of a fault plane (red line), usually showing a higher degree of deformation than the surrounding rocks (van der Zee, 2002).

(d) Fault gouge consisting of parallel strands, with telescoping of the individual layers (van der Zee, 2002).

(e) Fault gouge with lateral injection of a weak layer (this paper).

(f) Fault gouge formed by the process of preferred smear of the soft layer (van der Zee, 2002).

(g) Fault gouge formed by disruption of the stronger layer followed by mixing of the fragments.

(h) The brittle end member fault, with open fractures, developing preferentially in releasing sections.

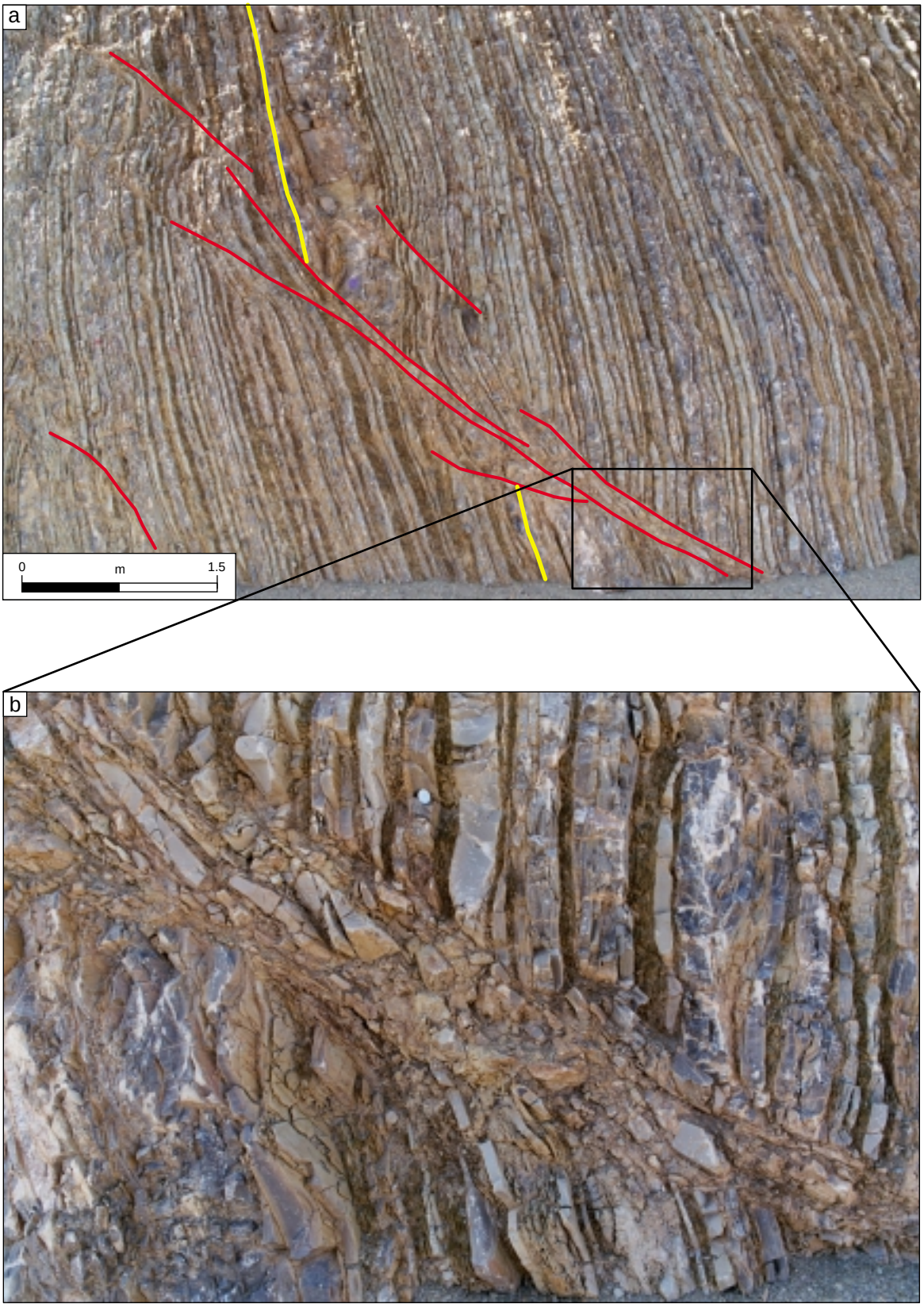

Figure 4: Field example of the fault gouge structures illustrated in Figure 3g, in an outcrop of deformed Huwasina sediments near Izki, Oman. (a) Overview of the structure, with a steeply dipping limestone-shale sequence in the overturned limb of a thrust-related anticline. (b) detail of the fault zone, in the area shown in (a). This structure is interpreted to have formed by disruption of the brittle limestone and the subsequent mixing of these fragments with the shale that has become softened by mechanical reworking.

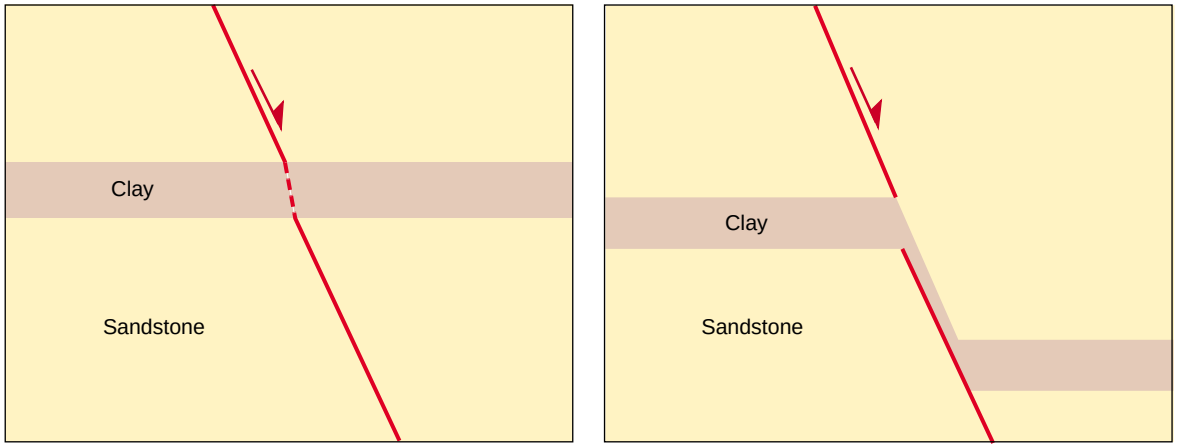

Figure 5: Schematic illustration of the injection of clay into a releasing step in a fault zone.

(1998) and van der Zee (2002). The thinly layered sequence consists of 85 % sand and 15 % clay. This outcrop is usually interpreted as an exhumed part of a collapsed crest and it contains a large number of small faults forming a wide range of clay smear structures (Figure 6). The major deformation occurred after burial to a depth less than 1,000 m, and is extensional, producing abundant normal faults with throws up to 50 m. Figure 7 is a small-scale example of lateral clay injection structure, where an approximately 5 cm thick clay bed is stepwise thinned towards the fault zone. The clay, which was originally in this bed is reallocated into the fault zone. The flow of this clay is associated with a disruption of the sandstone bed next to the clay.

Another example is Figure 8. Here, two faults are visible. On the left, a 30 cm thick clay bed is offset by a fault with a throw of 30 cm. The fault contains a thick layer of clay. On the right side of the outcrop, a fault with a much smaller offset shows how this structure may have originated in a releasing step across the clay layer.

Hambach, Germany

The opencast lignite mine near Hambach, Germany (Rheinbraun AG) is located in a layered package of Miocene age, consisting of sand, clay and lignite. The faults described in this paper are post-sedimentary, associated with regional extension during the Miocene-Pliocene (Knufinke and Kothen, 1997). The present depth of the sediments (400 m) is also the maximum burial depth. Early joints are present in the lignite. Clay layers have a thickness of 1 m and are frequently incorporated into the fault gouge. The structure shown in Figure 9 is from the fault called "Elsdorferbuergersprung 1.1". This fault, with an offset of approximately 10 m, was studied in a cut

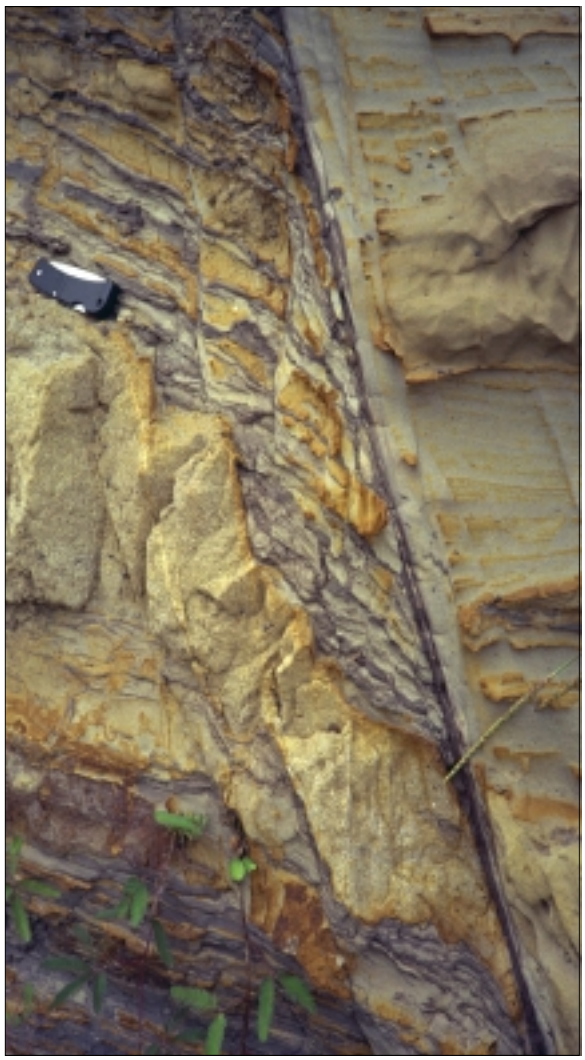

Figure 6: Normal fault in a deltaic sand-mudstone sequence, Airport road outcrop, Sarawak, Malaysia. Note the continuous seam of clay in the fault gouge, making this section of the fault a good lateral seal. However, the processes which led to the formation of this clay smear are not clear.

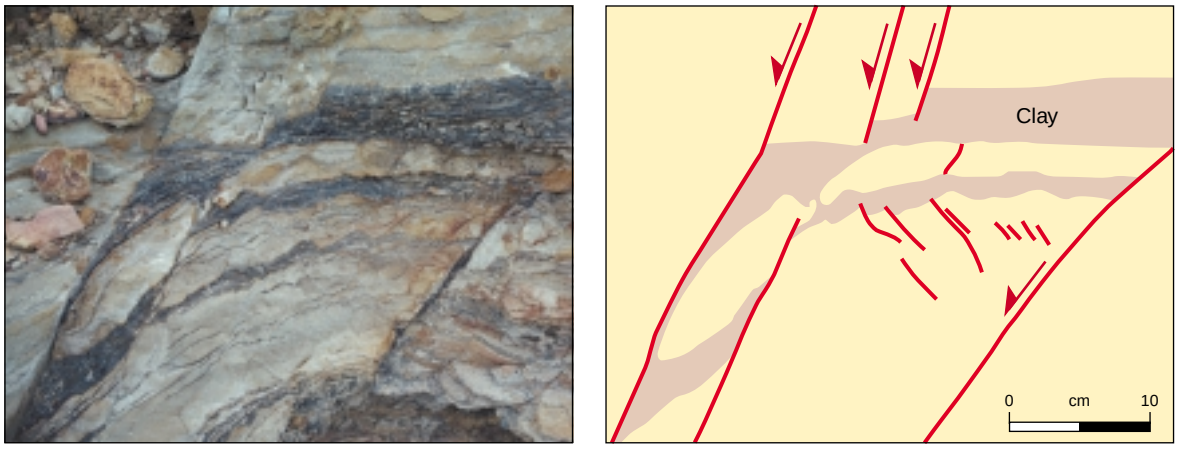

Figure 7: Example of small-scale lateral clay injection structure. The clay layer is step-wise thinned towards the fault at the left. The clay is reallocated into the fault zone. The sandstone bed in the clay layer is disrupted, and is surrounded by a clay matrix in the fault zone. Airport road outcrop, Sarawak.

perpendicular to the fault strike. The fault brings a lignite bed in juxtaposition with another lignite layer, and the fault gouge between the two consists of sheared lignite and clay. Two clay layers which are involved in the faulting can be observed in the outcrop; of these two the lower, approximately 1 m thick clay bed can be followed for at least 5 m outside the fault zone. Along this traverse it is constant in thickness. On approaching the fault the clay layer becomes thinner in two steps. From the point where the layer enters the fault zone, it can be followed for at least 1.5 m inside the gouge (to the bottom of the outcrop).

Kinematic Model

To explain the kinematics of the process, we expand the model proposed by Lehner and Pilaar (1997). The first stage (Figure 10a) is a fault with a releasing bend located inside the clay layer. There are many possibilities to create such a releasing step in the clay bed, one of which is in an upward propagating fault as proposed by Lehner and Pilaar (1997). In this study we do not attempt to explain the details of how these faults form, rather we start our analysis assuming that this releasing step has already formed. Further discussion of this process is presented in the discussion section of the paper. With ongoing throw, this releasing step develops into a pull-apart structure in the clay layer. This void is filled with clay laterally injected from the clay layer, and with further deformation this produces an abnormally thick zone of clay in the fault. In stage 2 (Figure 10b) with further offset, the thinning of the clay layer causes a slight bending of the top sand layer. After only a small amount of homogeneous

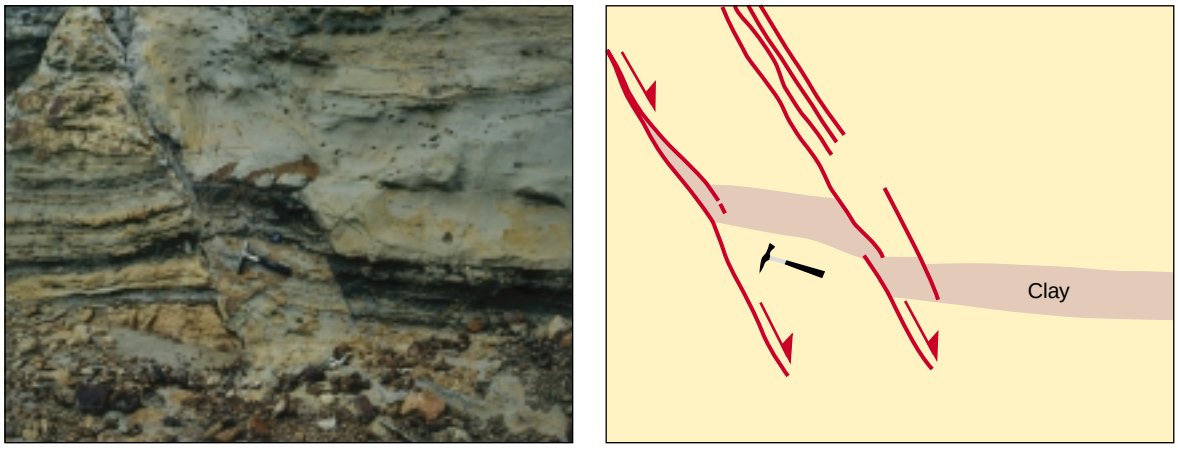

Figure 8: Field example of a releasing step in a clay layer, Airport road outcrop, Sarawak.

deformation, deformation in the sand layer is localized, and a second fault initiates to form a "squeezing block". In agreement with field observations we assume in our model that this second fault initiates approximately 0.5 to 1 times the clay bed's thickness away from the main fault. Downward movement of the squeezing block causes the lateral stepwise thinning of the clay layer towards the fault zone and injection of the clay into the fault (Figure 10c). With ongoing deformation more faults may initiate, forming multiple squeezing blocks. We note in passing that this is a passive mode of clay injection, which requires the presence of a releasing bend located in the clay layer. Active injection, whereby the clay is "pushing" other material away to force itself into the fault zone (cf. Meier, 1993) is not part of this model, and we cannot see any mechanical basis for such a process.

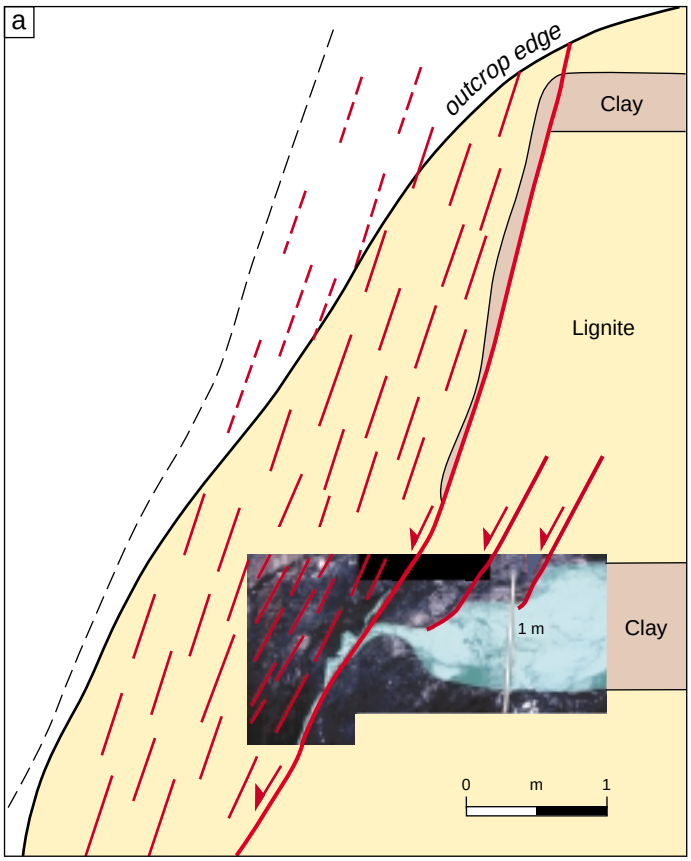

Figure 9: Profile of a clay injection in Tagebau Hambach, Germany (Elsdorferbuergersprung 1.1). This fault zone consists of two splays, only the eastern splay is investigated. Note the stepwise thinning of the clay layer towards the fault. This is direct evidence for the lateral injection process.

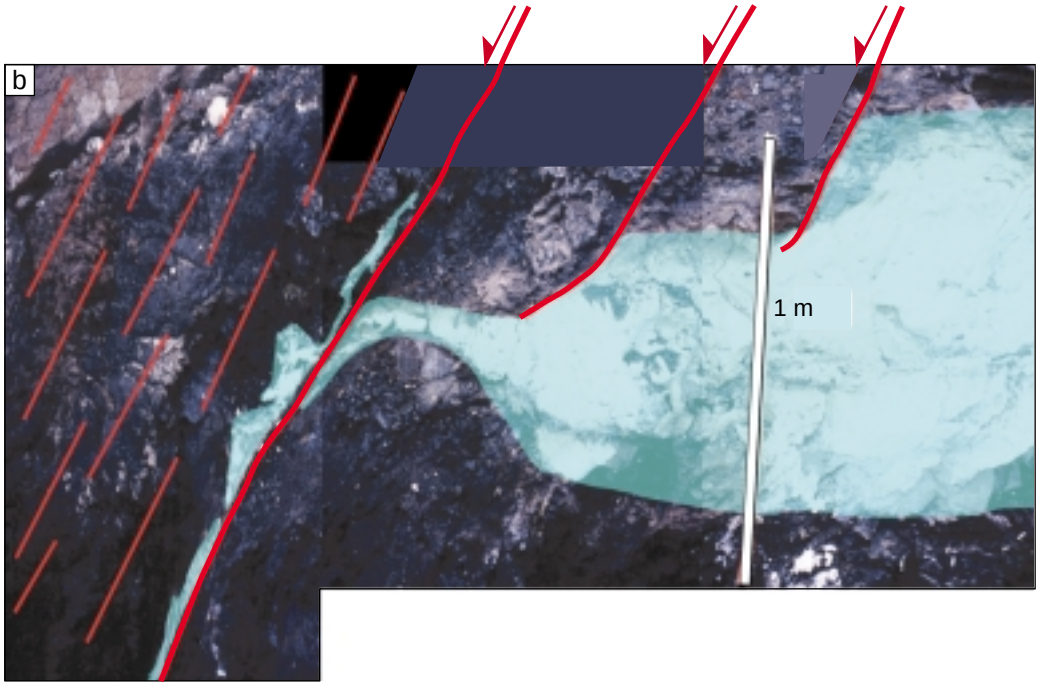

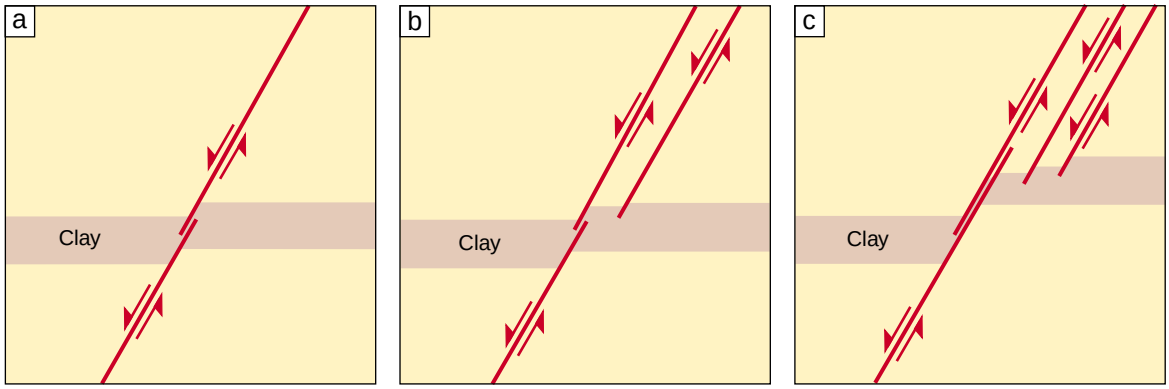

Figure 10: Kinematic model of lateral clay injection based on the kinematics shown in Figure 5.

MECHANICAL ANALYSIS

In this section we explore the dynamics of the kinematic model explained above, to quantify the important mechanical parameters involved. First we present a simple geomechanical model aiming to clarify the main elements of the system. More detailed analysis requires numerical techniques, these were done using the finite element package ABAQUS (Hibbit, Karlsson and Sorensen, Inc.).

A Simplified Model in Mohr space

To illustrate the main mechanical aspects of this system, we present a simple model using Mohr diagrams (Figure 11). The structural evolution is at a stage that the fault has just formed across the whole area considered, but the fault throw is still very small and the two sides of the fault in the releasing bend have been partially unloaded but have not yet separated. We now consider a point (A) in the releasing bend. The maximum principle effective stress (σ'_1) approximately equals the overburden load. The minimum principle effective stress (σ'_3) in this point is approximately horizontal, and is progressively reduced by the fault movement. In Mohr space this results in the Mohr circle with its right leg fixed and its left leg moving to the left (Figure 11). At this point there are two possibilities.

(I) The yield envelope is reached before $\sigma'_3 = 0$, and plastic flow of the clay towards the pull-apart structure is initiated.
(II) In a more cohesive clay, the yield envelope is not reached before $\sigma'_3 = 0$. The pull-apart structure will open because the clay layer can support the vertical load without becoming plastic. Therefore there will be no injection, but the formation of a dilatant void instead. In this situation other processes may take place such as vein growth, Hilgers and Urai (2000).

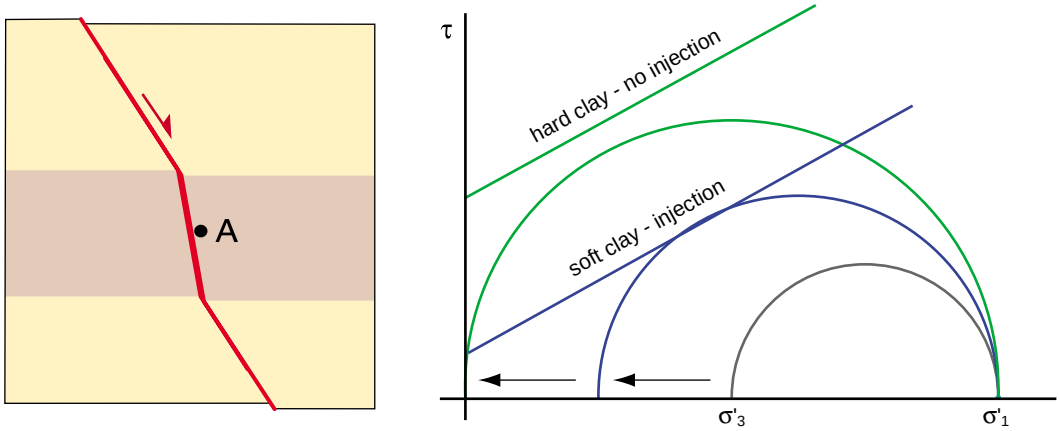

Figure 11: Schematic sketch of the stress evolution, in Mohr space, of a point (A) in the clay layer in a releasing bend of a normal fault.

For the case of a linear Mohr-Coulomb plasticity criterion the condition for the onset of lateral injection can be written by:

$$C = \frac{\sigma'_1 (1 - \sin \phi)}{(2 \cos \phi)} \qquad \text{Equation 1}$$

where C is cohesion (MPa), σ'_1 is the maximum principle effective stress (MPa) and ϕ is internal friction angle (degrees). Equation (1) is a first-order description of the conditions required for injection of clay. It contains a description of the interdependence of in-situ stress and rock strength. The usefulness of this equation comes from the fact that all the parameters involved can be in principle obtained from wire line log and cuttings data. Therefore this relationship can be used to predict the onset of clay injection in the subsurface.

Finite Element Modeling

The limitation of equation (1) is that it does not describe the heterogeneous stress field around a releasing step which is established after the first motion of the fault. To evaluate this, numerical methods are required. The method in this study uses finite element models built using the ABAQUS package.

Mesh and Material Properties

The continuum part of all models consist of 4-noded solid elements (CPE4, HKS, 1998), which were assigned elastoplastic (Mohr-Coulomb plasticity with cohesion hardening) mechanical properties. The faults are predefined and represented by finite-sliding, surface-based mechanical-contact formulations including a Coulomb friction model (Figure 12). The central part of the model is refined to get the finest mesh near the fault. Initial stresses were set to isotropic ($\sigma'_1 = \sigma'_3$). The model is divided in three layers and represents one clay layer between two sand layers. Their mechanical properties are listed in Table 1. In these models the sand was always stronger than the clay. The material properties with high cohesion for the sand, lower cohesion for the clay and a cohesionless fault represent conditions at a depth of approximately 4 km, in a sediment that shows a significant weakening after yielding.

Two different finite element meshes were built based on the kinematic model described above. Both meshes are rectangular with a releasing bend in the fault inside the clay layer. In the first model this is the only fault, in the second model a second fault was incorporated to represent the initiation of the squeezing block.

Table 1:
Input variables for the finite element models. E = Youngs modulus, C = Cohesion, ϕ = Internal friction angle, ψ = Dilatancy angle, υ = Poissons ratio

model	E (GPa)	initial C sand (MPa)	initial C clay (MPa)	C after 20% deform. (MPa)	ϕ sand (°)	ϕ clay (°)	ψ (°)	υ (–)	fault friction coeff.	initial stress (MPa)
1 fault	20	50	10	+1	30	10	0	0.3	0.1	50
2 faults	20	50	10-30	+1	30	10-30	0	0.3	0.1	50
sens. analyses	10	70	15-40	+0	30	5-35	0	0.3	0.1	70

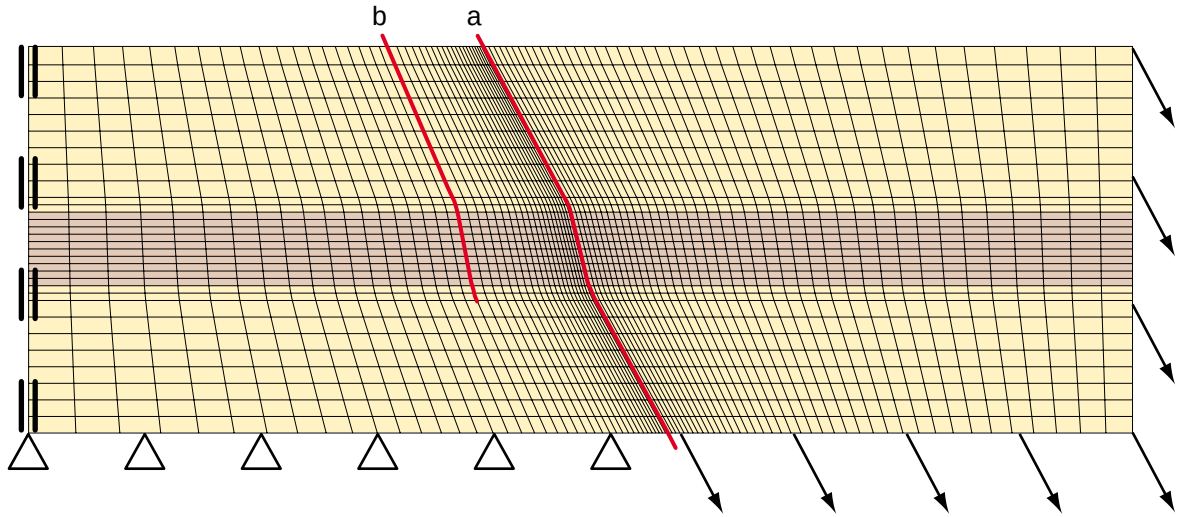

Figure 12: Mesh used for the finite element analyses. In the models with 1 fault, only fault (a) is present. In the models with a squeezing block, fault (b) is present also. The elements in the brown layer have "clay" properties and those in the yellow layer have "sand" properties. After the initial stress field is built up, the lower and right boundary of the hanging wall are moved along the pre-described path shown by arrows.

Calculation Procedure

The analyses are run in two steps. In the first step external distributed loads (HKS 1998) were applied on the sides and top of the model to invoke the initial stress (for details see Table 1). In the second step a pre-described displacement parallel to the direction of the flat part of the fault was imposed on the model. During this second step, the principal stresses in the centers of selected elements were collected for tabular output.

Results

The Onset of Clay Injection

The first aim of the analyses was to determine if by suitable choice of the input parameters the lateral injection of the clay could be turned on or off. This is indeed the case and Figure 13 is an example of two models: one with injection and one without injection. The onset of injection can be monitored by the occurrence of plasticity in the clay layer near the pull-apart structure. If there is no plasticity in the clay layer, then no injection has occured. Figure 13a shows that the largest magnitude of strain is observed near the sand-clay interface. This is due to the 'plug' shape of the flow profile of the plastic clay which has a rheology with a highly nonlinear dependence of strain rate on deviatoric stress (Turcotte and Schubert, 1982; van der Zee, 2002). We also note that most of the clay initially injected into the fault comes from the footwall of the fault.

Displacement contours in models with or without clay injection are shown in Figure 14. This Figure shows, in the case of injection, that the sand above the clay bends downwards, and correspondingly the clay moves laterally into the releasing step. Figure 15 shows the corresponding changes in stress: both σ'_1 and σ'_3 decrease around the releasing step, as expected. This perturbation in the stress field initially does not reach far into the clay layer, and initial injection of the clay is a process in the immediate vicinity of the fault.

The evolution of stresses in the middle of the releasing section is shown in Figure 16. Here, calculated stress changes in selected elements are plotted in a diagram of maximum shear stress τ_m vs. mean effective stress σ'_m defined as

$$\tau_m = 0.5\,(\sigma'_1 - \sigma'_3) \text{ and } \sigma'_m = 0.5\,(\sigma'_1 + \sigma'_3) \text{ and therefore } \tau_m = C \cos\phi + \sigma_m \sin\phi.$$

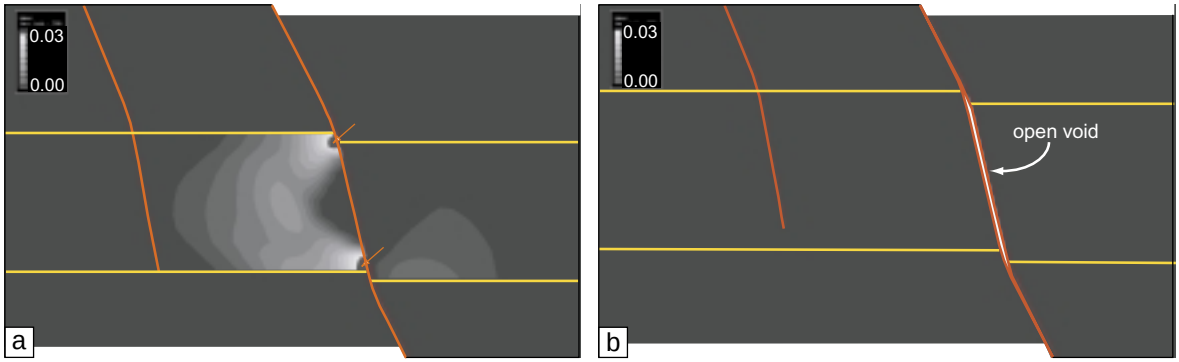

Figure 13: Contour plots of magnitude of plastic strain. (a) Injection, the clay layer deforms plastically, no loss of contact of the fault plane. Arrows indicate elements which are strongly deformed, strain values fall outside the contour range. (b) A stronger clay can support the overburden, opening of the pull-apart structure leads to loss of contact between the two sides of the fault. No plastic deformation of the clay is observed.

Figure 16 shows an experiment with injection and one without. A series of elements in the middle of the clay layer of the left block are plotted. In Figure 16a, the elements far from the fault show only a small change in stress state, whereas the ones closer to the fault structure have a stress path towards the Mohr-Coloumb yield envelope. During plastic deformation the stresses remain on the failure envelope, as expected. In Figure 16b the stress path is similar (the initial elastic deformation of both models is very similar, but the stresses do not reach the yield envelope).

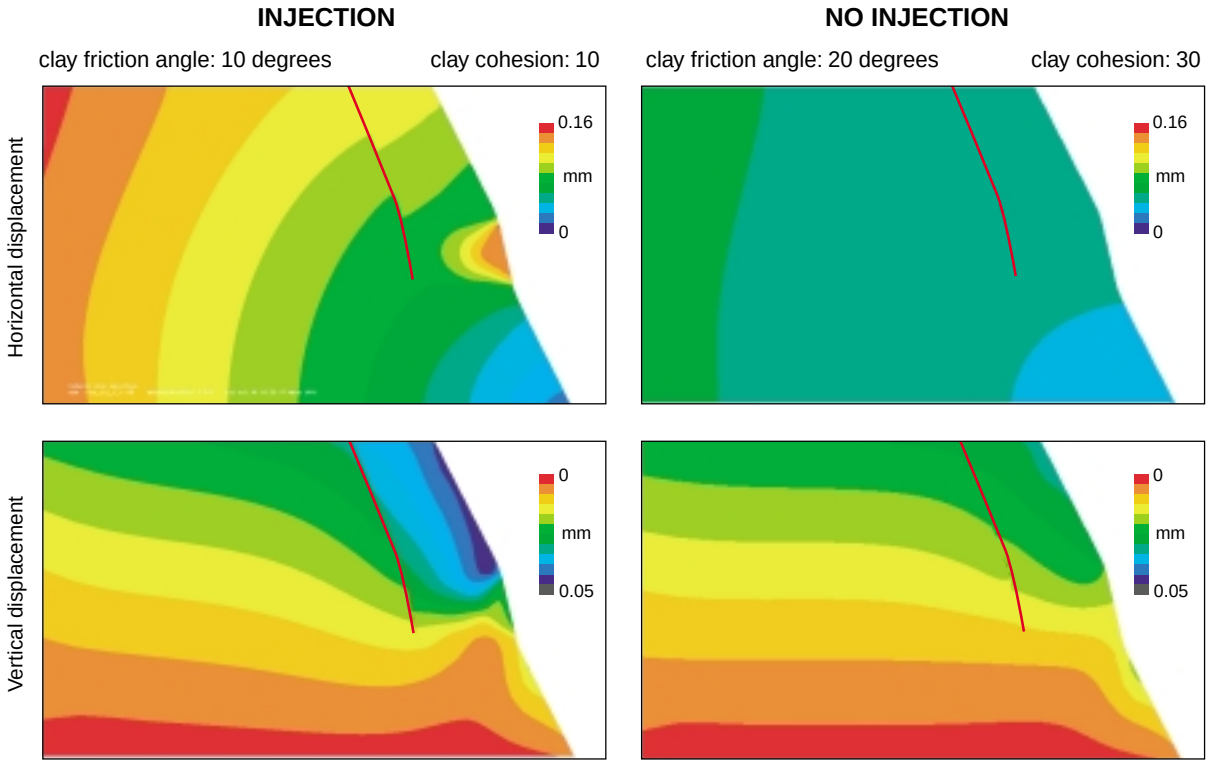

Figure 14: Contours of vertical and horizontal displacement. Vertical movement of the squeezing block, and horizontal movement of the clay is observed in the case of lateral clay injection. In the case of no injection only small, elastic displacements are observed. (Note that we left out the hanging wall block intentionally, because the displacements in this block are much larger than those in the footwall block.)

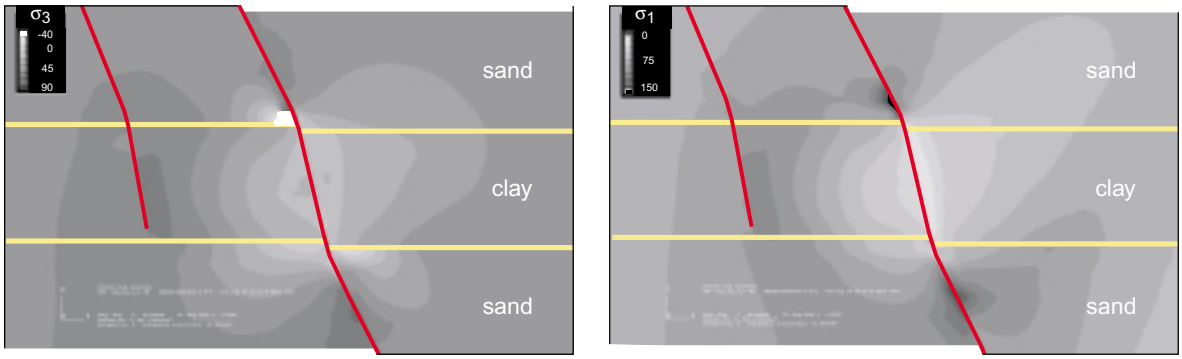

Figure 15: Contours of maximum and minimum principal stresses (MPa) of the same model as shown in Figure 13. A clear decrease of both principle stresses is observed near the pull-apart structure. Note that compressive stresses are positive.

To investigate the influence of different parameters on the system, we performed a sensitivity analysis. A series of numerical experiments were conducted with different values of friction angle and cohesion for the clay. The results are plotted in a cohesion vs. friction-angle graph, indicating the occurrence of clay injection (Figure 17). It can be seen that there is a clear distinction between the two conditions, separated by a curved boundary. An interesting observation (not shown in this graph) is that points far in the field of injection show similar behavior to conditions closer to the boundary. Thus the numerical analysis does not indicate more rapid injection with increasingly soft clay. The significance of this result will be further explored in the sandbox models presented below.

A plot of equation (1) in Figure 17 shows that although the results of Finite Element modeling are quite complex, the simple single-point Mohr-Coloumb-model of Figure 11 does capture most of the essential elements of the system's behavior. The boundaries between the two fields, as defined by both methods are in good general agreement, with somewhat higher friction angle dependence in the finite element results. The largest difference between the Finite Element analyses and the simple model is that in the Finite Element models not only σ'_3 is reduced, but also σ'_1, whereas in the simple model σ'_1 stays constant. Therefore the changes in Mohr circle depicted in Figure 11 are slightly different, even for a point in the Finite Element model which is in the position of point A in Figure 11.

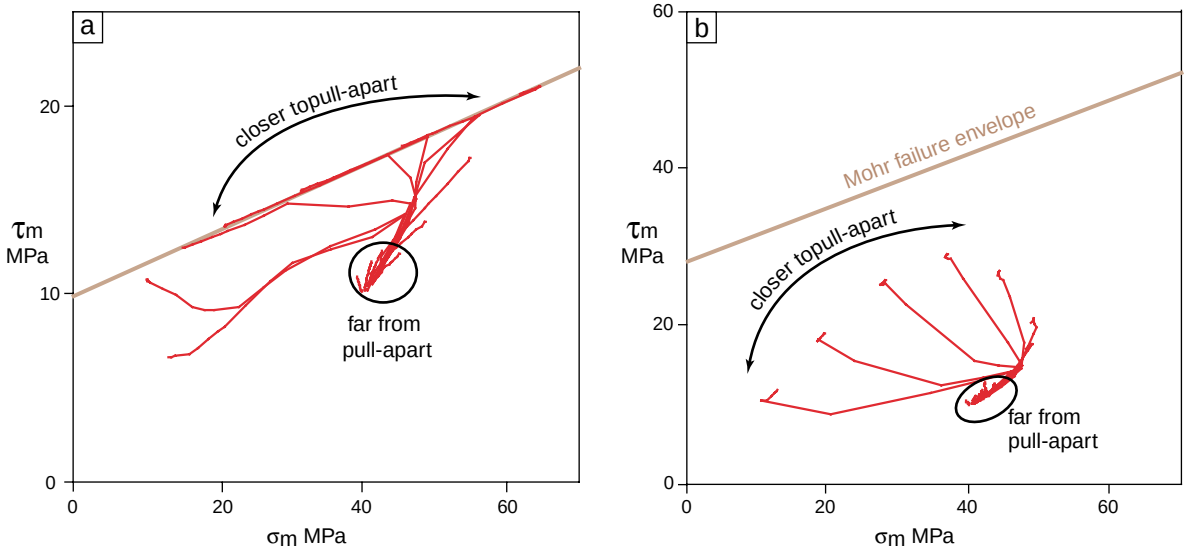

Figure 16: Stress paths of selected elements in the clay layer. a) In the case of injection, the elements close to the pull-apart reach the Mohr failure envelope, whereas the stress field in the elements further away from the pull-apart structure does not change significantly. b) Without injection, shows the same pattern as (a), but the higher cohesion prevents plastic deformation of the elements.

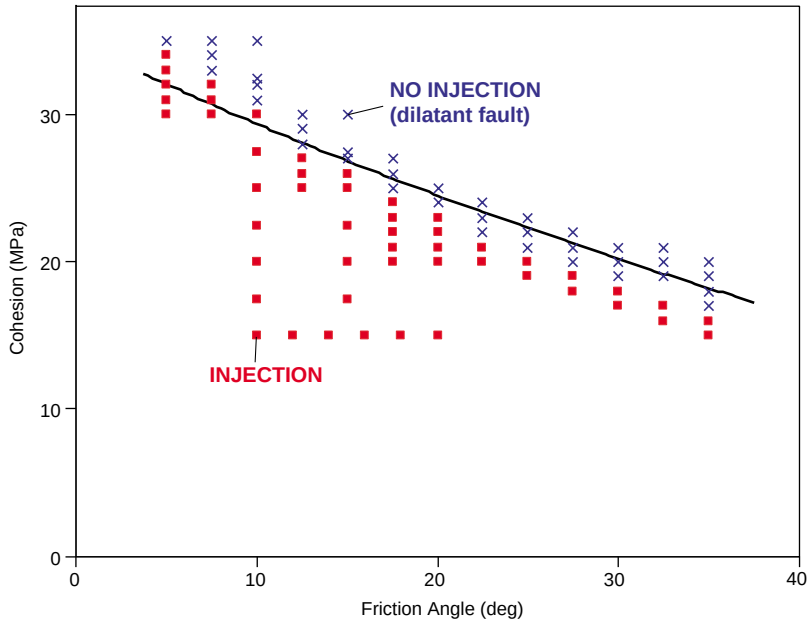

Figure 17: Cohesion vs. friction angle graph for a series of analyses with different values for Cohesion and friction angle. Squares are the combinations where injection is observed, crosses are related to an open pull-apart structure (no plasticity in clay layer). Line represents Equation 1. It can be seen that although the finite element results are quite complex, the basic mechanical analysis formulated in Equation 1 does describes the boundary between the two fields reasonably well.

Influence of the Squeezing Block

In a number of models we added an additional interface element in the footwall, to investigate the effect of a squeezing block. In both meshes the material properties were the same, and the clay was soft enough to flow into the pull-apart structure. Interestingly, we found almost no difference between the models. In both cases (with and without second fault in the model) the clay injects predominantly from the footwall layer, and the calculated onset of injection is also consistent with Equation 1. In more detail, without a squeezing block the region of plasticity in the clay layer is larger than in the case with the squeezing block, where the plastic region in the clay layer is controlled by the width of the squeezing block. This suggests that while the onset of injection is not dependent on the presence of a squeezing block, differences may arise at larger offsets. Unfortunately, numerical convergence problems prevent the continuation of this analysis to large fault displacements.

ANALOGUE MODELING

Because of the limitations of the numerical scheme at large fault displacements, we studied clay injection at large displacements using analogue modeling techniques. This technique allows study of the kinematics of clay injection at a much higher strain than currently possible with numerical techniques. In this section of the paper the experimental results are summarized, and compared with the results of the numerical modeling.

Method

The analogue models were constructed using horizontal layers of two distinct materials, a ductile clay analogue and dry sand, overlying a basement fault dipping at 45 degrees. Movement on the pre-existing basement fault creates normal faulting in the multi-layered sedimentary overburden, a structure which has been studied extensively in the past (Horsfield, 1977; Richard, 1991). Dry sand shows brittle behavior and is an appropriate analogue for competent rocks such as sand and sandstones. This Mohr-Coloumb material has a small but finite cohesion (Schellart, 2000) and a friction angle of around 35 degrees. The ductile material (silicone putty) traditionally used in analogue modeling is unsuitable for our experiments: while silicone putty is essentially a Newtonian viscous fluid, clay under natural conditions is a plastic material: its deformation is rate-independent under fully drained conditions. In experiments simulating clay injection, the large changes in shear rate due to the movement of the soft phase into thin channels can be expected to result in kinematics of silicone putty, which are not representative of the clay prototype. As an alternative we selected a

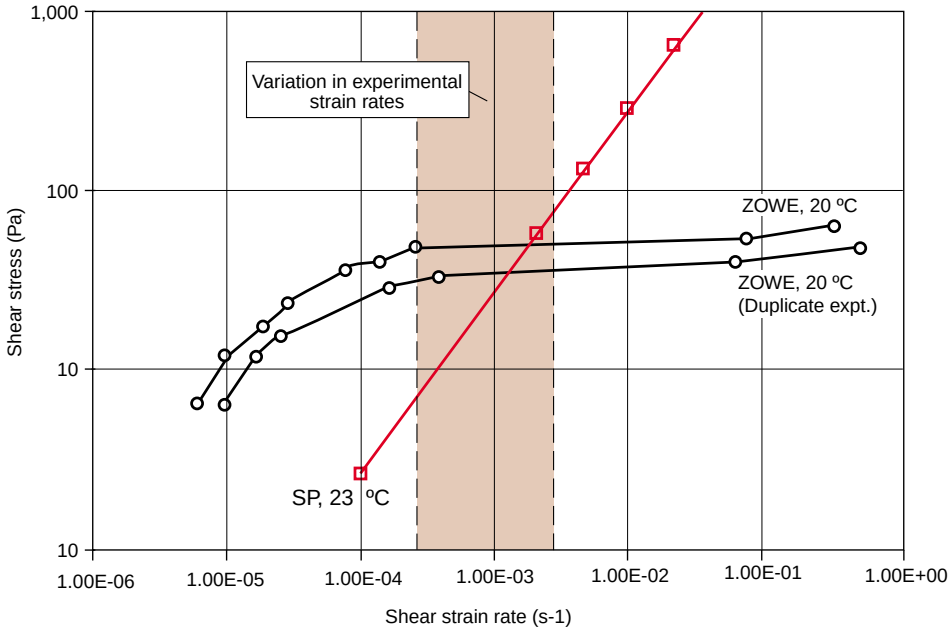

Figure 18: Rheological properties of ZOWE and silicone putty (SP), as measured in a cone- and plate rheometer at room temperature.

soft, commercially available oil-water emulsion, hereafter called ZOWE (www.zwitsal.com) for this study. It has a low density (around 1,000 kg/cm^3) and is to a first order an elastoplastic material. The substance is stiff, Young's modulus is in the order of a few kPa, and it can be readily colored using standard dyes. The yield strength of the material is around 20 Pa, which makes it a suitable model material for clay in a scaled model of about 10 cm size. One of the important properties of ZOWE is that it mixes very little with sand and does not form a strong boundary layer. Mixing may produce artefacts, which have been rarely discussed in the literature on silicone-sand experiments. To obtain more detailed information on material properties, the room temperature rheology of ZOWE and silicone putty were measured in a cone- and plate rheometer. Results are shown in Figure 18, in a plot of steady-state shear stress versus the corresponding shear strain rate. It can be seen that at the strain rates relevant for our experiments the flow stress of ZOWE is essentially rate-independent: it is an elastoplastic material. At much lower rates the flow stress drops. This may be due to the rearrangement of the internal structure of the material to form a water-rich film at the boundaries (Goshawk and Binding, 1998). This interpretation is also supported by the long-term shape stability (days) of small pyramid-shaped peaks of the material, which do not flow at all at flow stresses below 5 Pa. Therefore the drop in flow stress shown in the diagram is interpreted to be not representative to bulk flow of the material. In summary, although the fine details of the rheologies are complex (Jogun and Zukoski, 1999; Pignon and Piau, 1998), ZOWE is to a first order a suitable analogue for scaled modeling of the deformation of soft clays.

Results

We compare a number of models identical in all aspects except for the thickness of the overburden of the ZOWE layer. We present results for a thin and thick overburden, 1.5 cm and 9.5 cm thick respectively.

Thin Overburden (1.5 cm)

In models with a thin overburden, a thin smear was created along the fault zone (Figure 19 a,b). The ZOWE in the hanging wall was sheared and dragged along the fault creating a continuous and asymmetric smear. Detailed examination of the experiments shows that with increasing deformation, the smear becomes discontinuous; no ZOWE is injected from the unfaulted part of the layer into the fault zone. This observation was independent of the ZOWE thickness layer which varied from 0.5 to 2 cm.

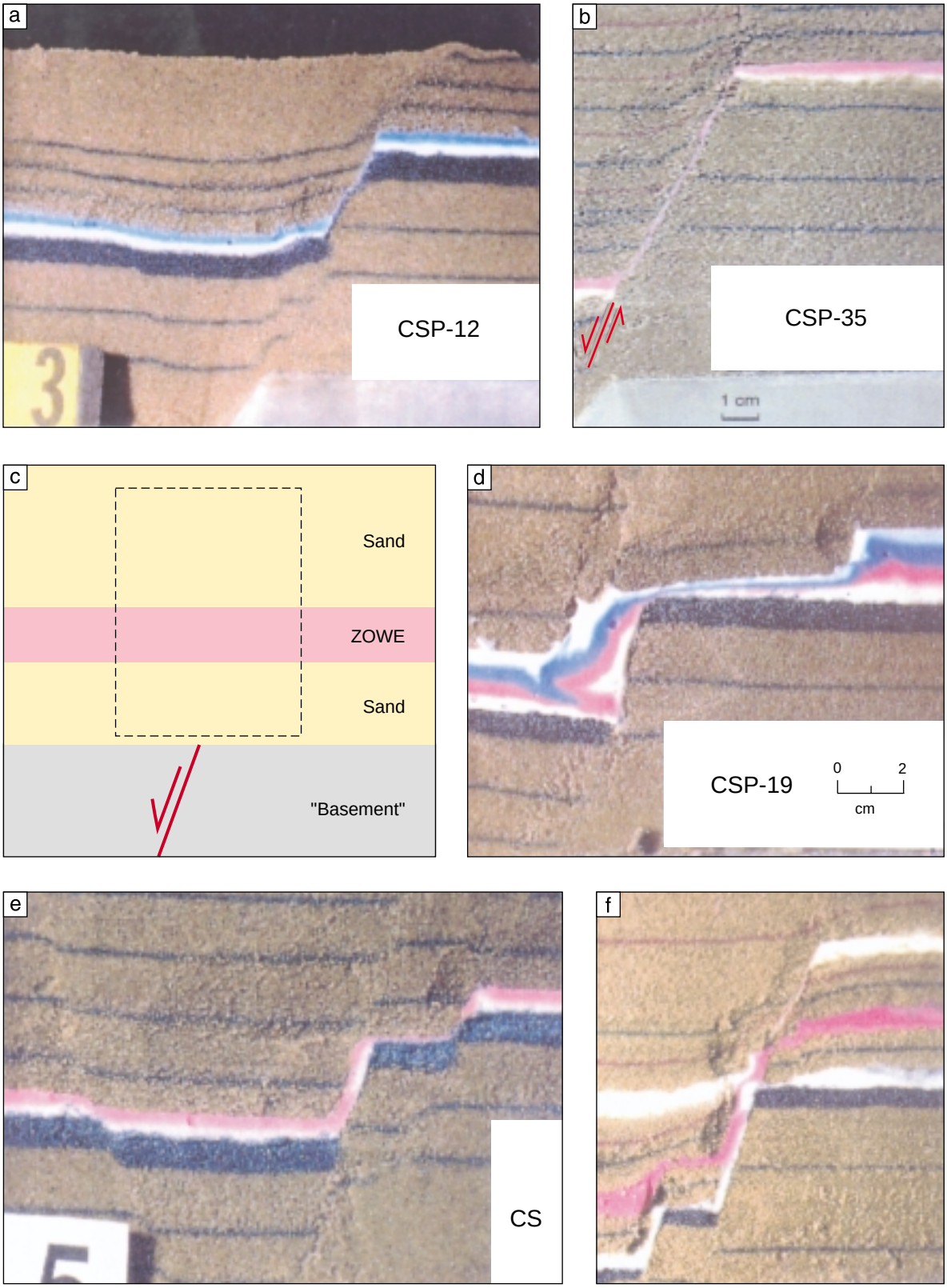

Figure 19: Results of sandbox experiments with sand and ZOWE. (a, b) thin overburden (1.5 cm), no clay injection; (c) schematic drawing of the experimental setup; (d, e) thick overburden (9.5 cm), extensive lateral injection and formation of squeezing block similar to Figure 9; and (f) experiment with three ZOWE layers where the two deeper layers develop a squeezing block but the upper layer (thin overburden) does not. In (a), (b), (c) and (f) the ZOWE thickness layer was 0.5 cm; in (d) it was 2 cm.

Thick Overburden (9.5 cm)

In this model, a thick zone of ZOWE was created by injection into the fault zone (Figure 19c,d). The structures observed resemble those observed in the field. The basement fault formed a releasing step in the ZOWE layer, and a second fault was initiated to form the squeezing block. The vertical displacement imposed on the basement fault was equally accommodated by the two normal faults. The ZOWE below the squeezing block can be completely injected into the fault plane, thinning the ZOWE in the footwall bed and thickening the smear in the fault plane. The smear was asymmetrical in the sense that its thickness was variable, and the main source for the smear was the footwall layer. The formation of the squeezing block was independent from the ZOWE thickness layer which varied from 0.5 cm to 2 cm.

Mechanical Analysis

The major differences between the thin and thick overburden cases can be explained by considering the contrast in strength between the sand and the ZOWE, and the ratio of strength and overburden stress in the ZOWE. The yield stress of the ZOWE is independent of depth. Consequently, for a thick overburden, the vertical stress to drive flow of ZOWE, and the strength contrast between sand and ZOWE is much more pronounced than for a thin overburden. At a certain overburden thickness the squeezing block is spontaneously initiated in the footwall, leading to injection of ZOWE. A surprising result was that using Equation 1, the onset of injection would be predicted for both experiments. The difference is that for a thin overburden, in our experiments the releasing section is not spontaneously formed in the ZOWE layer and therefore injection does not occur. This process of the formation of the releasing bend in the clay layer is poorly understood and needs further study. We will discuss it further in the discussion section of the paper.

Mechanical Clay Injection Potential

Based on the model for lateral clay injection described above, a criterion for Mechanical Clay Injection Potential (MCIP) was defined based on Equation 1, as follows:

$$\text{MCIP} = \frac{\sigma'_1 (1 - \sin\phi)}{(2 \cos \phi)\, C} \qquad \text{Equation 2}$$

This criterion predicts the tendency of lateral clay injection into a pull- apart structure in the fault. Its attractiveness lies in the possibility of calculating it from wireline log and cuttings data. Thus, MCIP depends on:

1) Strength ratio of sand and clay at a depth (is the clay weaker than the sand?).

2) Strength of clay versus effective vertical stress (does the clay flow under the overburden load?).

The algorithm works as follows: (1) from compressional and shear acoustic velocities (V_s and / or V_p) the unconfined compressive strength of shale is estimated, and from surface area data of cuttings the internal friction angle is estimated, based on equations presented in Urai (1995) and Urai et al. (1997). For a given depth and associated overburden pressure calculated from density logs, this is used to calculate MCIP. Figure 20 is an example of such a MCIP log.

We note here that while this tool only predicts the tendency of the clay to flow into releasing sections of a fault plane, it says nothing about the initiation of a squeezing block in the hanging wall, and is thus insufficient to fully quantify the presence of clay in the fault. For this, in addition to the mechanical constraints, the kinematic boundary conditions are important, such as the presence of a pull-apart structure in the clay layer. This analysis is outside the scope of the paper. However, one might imagine that for this purpose a Kinematical Clay injection Potential (KCIP) may be defined - this is subject of our ongoing study. The analogue models serve well to illustrate the importance of these kinematic parameters, but a full quantification needs more work.

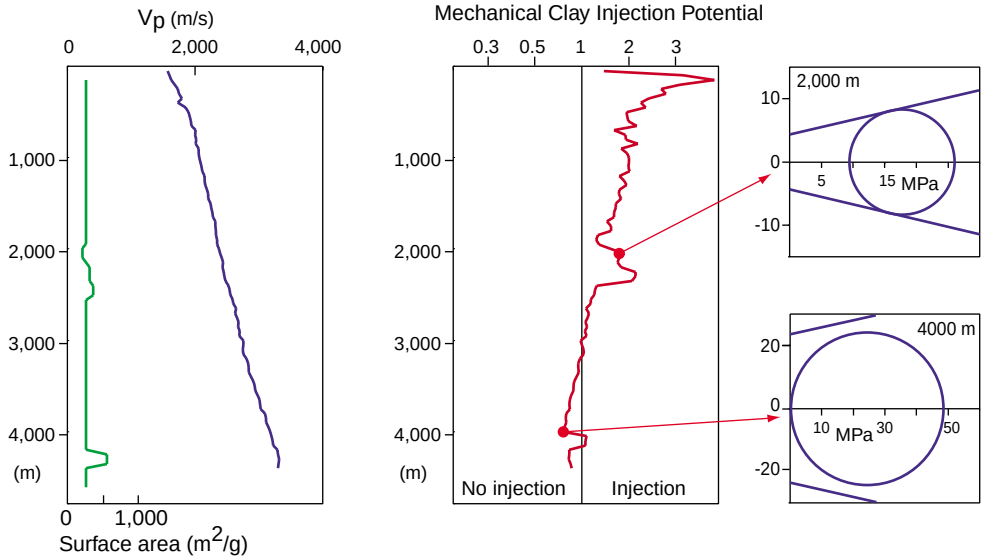

Figure 20: Example of a Mechanical Clay Injection Potential log calculated from a typical velocity depth trend in a Tertiary delta. Plotted are only the calculated points in the shale layers, based on a SGR cutoff criterion. In the whole section we assume that sand is stronger than the clay. Input parameters are V_p and/or V_s, and surface area. Output is a graph showing the mechanical tendency of the clay to flow towards a pull-apart structure. Note the decreasing trend of MCIP with depth.

The two criteria presented above form a basis for improvement of the conventional clay smear prediction tools such as SGR which are based on the bulk clay content of the faulted section (obviously, if there is no clay present in the formation faulted, then no clay will be present in the gouge). Thus, we propose the definition of the parameter CIF (Clay In Fault) as the true clay fraction in a fault at a given location. The arguments above can be summarized by the following equation:

$$CIF = KCIP * MCIP * SGR$$

where CIF is Clay In Fault, KCIP is the Kinematical Clay Injection Potential, and SGR is Shale Gouge Ratio (Fristad et al., 1997; Yielding 2002).

Recalling Figure 3, we note that if the calculation of CIF becomes possible in the future, one still has to address many other potentially important processes which occur in fault zones.

DISCUSSION

Releasing Step

As already mentioned in the descriptions of our kinematic model and analogue modeling, the genesis of the releasing step inside the clay layer is poorly understood. This structure was first described by Cloos (1930) in experimentally deformed clay-cakes and more recently by Richard (1991) for a viscous layer above a rigid basement block. Although it is not intuitively obvious how these structures can be generated (simple Mohr-Coulomb theory predicts that the fault is less steep in the clay layer with the lower friction angle); there are a number of kinematic models that predict such a structure to form: (1) upward propagation of a subhorizontal section of a fault's tip; (2) sideways propagation of a dip section of a fault's tip (Childs et al., 1996); and (3) coalescence of previously formed fault segments. Mechanically, these can be explained in two ways: either by the fact that irregularities are always present along a fault plane, and even if these are uncorrelated to lithology, releasing steps in the clay layer will be present at some locations, (together with releasing steps in the sand). The same argumentation holds for (3). Or the other possibility is that the presence of the clay layer preferentially induces a releasing step. For this, in case (1) Mandl (2000) showed with help of a Terzaghi's pole construction that this process could be mechanically feasible. Patton and Fletcher (1995) analyzed the

shape of a flexural bending in a layer above basement blocks with a 45 degree normal fault. They found that the position of the neutral point relative to the fault plane is shifted towards the downthrown block. When this "neutral point" is the place for fault initiation in the layers above, this would cause a releasing step (cf. Meier, 1993). Case (2) is much less understood, (cf. Kattenhorn et al., 2000) and needs further study.

A hint to the relationship of MCIP and the spontaneous initiation of the squeezing block may be provided by the observation in our sandbox models that for MCIP slightly higher than 1, (injection is already predicted by Equation 1) the fault moves without the formation of a releasing step. This does occur at higher values of MCIP. It may well be that for MCIP much higher than 1 the contrast in strength between the two layers becomes sufficiently large to allow initiation of a squeezing block. Therefore, although this is not shown by the numerical modeling, there is some theoretical basis to assume that progressively higher MCIP is associated with progressively higher probability of large amounts of clay being present in a fault zone.

In summary, at present, the mechanical explanation for a preferential development of releasing steps in clay layers remain hypothetical due to the lack of extensive field and experimental evidence. The evolution of these structures is subject of continuing study of our group.

Amount of Clay Incorporated in the Fault Gouge

In faults with very large offset, the fault gouge is deformed so strongly that no distinction can be made between a gouge formed by lateral clay injection, and gouges formed with other "clay smear" processes, where no clay enrichment of the fault gouge took place. Outcrop studies of these faults are not suitable for detailed study of the processes by which clay emplacement into faults occurs. This is the reason why our study concentrated on faults with small offsets: here a much clearer analysis of the system's evolution is possible.

Our kinematic model describes the initiation of squeezing blocks. As a consequence of this model, the maximum amount of clay available for lateral injection towards the fault is the volume of the clay below the block(s). This is different from the model proposed by Lehner and Pilaar (1997), where the sand layer above the clay layer bends during injection, and allows a larger volume of clay to be injected into the fault.

The use of semi-empirical "clay smear" tools was reviewed by Yielding et al. (1997) and Yielding (2002). The main difference between the Shale Gouge Ratio (SGR, Fristad et al., 1997) and Clay Smear Potential (CSP, Fulljames et al., 1997) is that with SGR the predicted amount of clay in the fault gouge is proportional to the amount of clay in the wallrock of the faulted interval, whereas CSP predicts clay to be dependent on the thickness of the source layers.

Our results show that lateral clay injection can result in more clay in the fault gouge than in the faulted interval of the wallrock, and that a prediction of this requires incorporating both the mechanics and kinematics of the system.

CONCLUSIONS

Lateral clay injection into a releasing bend of a fault may produce local enrichment of clay in the fault. This process is potentially important in most sedimentary sequences containing sands or carbonates interlayered with significant weak mudstone sections.

The mechanical requirement for this lateral injection process is that the ratio of mechanical strength of the mudstone and the in-situ effective stress is sufficiently low to allow flow of the mudstone into the releasing bend.

The tendency for this process can be quantified, using the MCIP algorithm, which is calculated based on wireline log and cuttings data. Fault seal predictions based on kinematic criteria, (SGR) can be improved by analysis of the mechanical properties of the wall rocks.

ACKNOWLEDGMENTS

We wish to thank Florian Lehner, Horst Neugebauer, Yves Leroy, Dick Nieuwland, Wolfgang Heidug, Christopher Wibberly, Christoph Horst, Henk Droste, John Temaga and Danny Soo for many illuminating discussions on clay rheology, numerical modeling, sandbox experiments and the geology of Sarawak and Oman. We thank Sarawak Shell Berhad for support with fieldwork in Miri, and Dr. S. Asmus of Rheinbraun AG for support with fieldwork in the Hambach opencast mine.

The authors thanks Peter Vrolÿk, Salim Al-Mahruqui and Joerg Mattner for reviews which greatly improved the manuscript. Financial support from the Deutsche Forschungsgemeinschaft (Grant UR 64-2) is gratefully acknowledged.

We thank the management of Shell International Exploration and Production Laboratories for permission to publish part of the results presented in this paper. The design and drafting of the final graphics was by Gulf PetroLink.

REFERENCES

Aydin, A. and Y. Eyal 2002. Anatomy of a normal fault with shale smear: implications for fault seal. American Association of Petroleum Geologists Bulletin, no. 86, p. 1367-1381.

Bouvier, J.D., C.H. Kaars-Sijpesteijn, D.F. Kluesner, C.C. Onyejekwe and R.C. van der Pal 1989. Three-dimensional seismic interpretation and fault sealing investigations, Nun River field, Nigeria. American Association of Petroleum Geologists Bulletin, no. 73, p. 1397-1414.

Burhannudinnur, M. and C.K. Morley 1997. Anatomy of growth fault zones in poorly lithified sandstones and shales: implications for reservoir studies and seismic interpretations. Part 1, outcrop study. Petroleum Geoscience, v. 3, p. 211-224.

van Buchem, F.S.P., P. Razin, P.W. Homewood, J.M. Philip, G.P. Eberli, J.-P. Platel, J. Roger, R. Eschard, G.M.J. Desaubliaux, T. Boisseau, J.-P. Leduc, R. Labourdette and S. Cantaloube 1996. High resolution sequence stratigraphy of the Natih Formation (Cenomanian/Turonian) in Northern Oman: Distribution of source rocks and reservoir facies: GeoArabia, v. 1, p. 65-91.

van Buchem, F.S.P., P. Razin, P.W. Homewood, H. Oterdoom, and J. Philip 2002, Stratigraphic organization of carbonate ramps and organic-rich intrashelf basins: Natih formation (middle Cretaceous) of northern Oman. AAPG bulletin, vol. 86, no. 1, 21- 54.

Childs, C., J. Watterson and J.J. Walsh 1996. A model for the structure and development of fault zones. Journal of the Geological Society of London, v. 153, p. 337-340.

Cloos, H. 1930. Zur experimentellen Tektonik. Geologische Rundschau 21, p. 353-367.

Fristad, T., A. Groth, G. Yielding and B. Freeman 1997. Quantitative fault seal prediction: a case study from Oseberg Syd. In, P. Moller-Pedersen and A.G. Koestler (Eds.), Hydrocarbon Seals. Norsh Petroleumforening Special Publication no. 7, p. 107-124.

Fulljames, J.R., L.J.J. Zijerveld and R.C.M.W. Franssen 1997. Fault seal processes: systematic analysis of fault seals over geological and production time scales. In, P. Moller-Pedersen and A.G. Koestler (Eds.), Hydrocarbon Seals. Norsh Petroleumforening Special Publication no. 7, p. 51-59.

Goshawk, J.A. and D.M. Binding 1998. Rheological phenomena occurring during the shearing flow of mayonnaise. Journal of Rheology, v. 42, no. 6.

Heynekamp, M.R., L.B. Goodwin, P.S. Mozley and W.C. Haneberg 1999. Controls on fault-zone architecture in poorly lithified sediments, Rio Grande rift, New Mexico: implications for fault-zone permeability and fluid flow. In, W.C. Haneberg, P.S. Mozley, J.C. Moore and L.B. Goodwin (Eds.), Faults and Subsurface Fluid Flow in the Shallow Crust. Geophysical Monograph 113, p. 27-49.

Hibitt, Karlsson and Sorensen Inc. 1998. ABAQUS/Standard User's Manual, v. I-III.

Hilgers, C. 2000. Vein growth in fractures - expiremental, numerical and real rock studies. 104 pp., Shaker verlag Aachen, ISBN 3-8265-7963-1.

Hilgers, C and Urai J.L. 2002. Experimental study of syntexiol vein growth during lateral flow in transmitted lgith, first results. Journal of Structural Geology, 24: 1029-1043.

Horsfield, W.T. 1977. An experimental approach to basement-controlled faulting. Geologie en Mijnbouw, v. 56, no. 4, p. 363-370.

Jogun, S.M. and C.F. Zukoski 1999. Rheology and microstructure of dense suspensions of plate-shaped colloidal particles. Journal of Rheology, v. 43, no. 4, p. 847-871.

Kattenhorn, S.A., A. Aydin and D.D. Pollard 2000. Joints at high angles to normal fault strike; an explanation using 3-D numerical models of fault-perturbed stress fields. Journal of Structural Geology, v. 22, no. 1, p. 1-23.

Knipe, R.J., Q.J. Fisher, G. Jones, M.R. Clennell, A.B. Farmer, A. Harrison, B. Kidd, E. McAllister, J.R. Porter and E.A. White 1997. Fault seal analysis: successful methodologies, application and future directions. In, P. Moller-Pedersen and A.G. Koestler (Eds.), Hydrocarbon Seals. Norsh Petroleumforening Special Publication no. 7, p. 15-38.

Knufinke, H.-U. and H. Kothen 1997. Die Tektonik der Niederrheinischen Bucht vor, während und nach der Hauptflözbildung. Braunkohle-Surface Mining, v. 49, p. 473-479.

Koledoye, B.A., A. Aydin and E. May 2000. Three-dimensional visualization of normal fault segmentation and its implication for fault growth. The Leading Edge, July 2000, p. 692-701.

Lehner, F. and W. Pilaar 1997. The emplacement of clay smears in syn-sedimentary normal faults: inference from field observations near Frechen, Germany. In, P. Moller-Pedersen and A.G. Koestler (Eds.), Hydrocarbon Seals. Norsh Petroleumforening Special Publication no. 7, p. 39-50.

Lesslar, P. and M. Wannier 1998. Destination Miri - a geological tour of northern Sarawak's national parks and giant caves. Ecomedia CD-Rom. http://www.sarawak.com.my/ecomedia software.

Lindsay, N.G., F.C. Murphy, J.J. Walsh and J. Watterson 1993. Outcrop studies of shale smears on fault surfaces. International Association of Sedimentologists, Special Publication no. 15, p. 113-123.

Logan, J.M. and K,A. Rauenzahn 1987. Frictional dependence of gouge mixtures of Quartz and Montmorillonite on velocity, composition and fabric. Tectonophysics, v. 144, p. 87-108.

Lupini, J.F., A.E. Skinner and P.R. Vaughan 1981. The drained residual strength of cohesive soils. Geotechnique, v. 31, no. 2, p. 181-213.

Mandl, G. 2000. Faulting in brittle rock: an introduction to mechanics of tectonic faulting. Springer-Verlag, Berlin, p. 434.

Meier, D. 1993. Abschiebungen: Geometrie und Entwicklung von Störungen im Extensionsregime. Enke Verlag, Stuttgart, p. 142.

Patton, T.L. and R.C. Fletcher 1995. Mathematical block-motion model for deformation of a layer above a 15 buried fault of arbitrary dip and sense of slip. Journal of Structural Geology, v. 17, no. 10, p. 1455-1472.

Pignon F. and J.-M. Piau 1998. Thixotropic behavior of clay dispersions: combinations of scattering and rheometric techniques. Journal of Rheology, v. 42, no. 6.

Rawling, G.C., L.B. Goodwin and J.L. Wilson 2001. Internal architecture, permeability structure, and hydrologic significance of contrasting fault-zone types. Geology, v. 29. no. 1, p. 43-46.

Richard, P. 1991. Experiments on faulting in a two-layer cover sequence overlying a reactivated basement fault with oblique-slip. Journal of Structural Geology, v. 13, no. 4, p. 459-469.

Richard, P.D., P.J.R. Nederlof, J.M.J. Terken and N. Al-Ruwehy 1998. Generation and retention of hydrocarbon in the Haushi Play, north Oman. GeoArabia, v. 3, no. 4, p. 493-506.

Schellart, W.P. 2000. Shear test results for cohesion and friction coefficients for different granular materials: scaling implications for their usage in analogue modeling. Tectonophysics, v. 324, p. 1-16.

Turcotte, D.L. and G. Schubert 1982. Geodynamics: applications of continuum physics to geological problems. John Wiley & Sons, New York, p. 450.

Urai, J.L. 1995. Brittle and ductile deformation of mudrocks. EOS, November 7, p. F565.

Urai, J.L., E. van Oort and W. van der Zee 1997. Correlations to predict the mechanical properties of mudrocks from wireline logs and drill cuttings. Annales Geophysicae, Supplement 1 to v. 15, p. C143.

Weber, K.J., G. Mandl, W.F. Pilaar, F. Lehner and R.G. Precious 1978. The role of faults in hydrocarbon migration and trapping in Nigerian growth fault structures. Proceedings of the 10th Annual Offshore Technology Conference.

Yielding, G., B. Freeman and D.T. Needham 1997. Quantitative fault seal prediction. American Association of Petroleum Geologists Bulletin, v. 81, no. 6, p. 897-917.

Yielding, G. 2003, Shale group ration - calibration by geohistory. In Hydrocarbon seal quantification, A.G. Koestler and R. Hunsdale (Eds). Norsh Petroleumforening special publications II, pp. 1-15.

van der Zee, W. 2002. Dynamics of fault gouge development in layered sand-clay sequences. Shaker Verlag Aachen, p. 155.

van der Zee, W. and J.L. Urai 2001. Fault zone evolution in layered sand-mudstone sequences. Hydrocarbon Seal Quantification Conference, Stavanger, Norway. Extended Abstracts, p. 171-180.

van der Zee, W., J.L. Urai and P.D. Richard 2000, Lateral clay injection into normal faults: Geophysical Reasearch Abstracts, v. 2, p. 25

ABOUT THE AUTHORS

Wouter van der Zee *works in the German office of GeoMechanics International Inc. He has a Msc in Structural geology on the dehydration behavior of gypsum under high pressure and temperature conditions, from the University of Utrecht, The Netherlands. In 2001 he received his PhD in structural geology at the Technical University of Aachen, Germany. His PhD subject was "Shale gouge development in layered sand-clay sequences" and included detailed fieldwork, numerical modeling and analogue modeling. Since 2002 he is working for GeoMechanics International Inc. in Mainz, Germany and is involved in software development and consulting projects concerning sand production prediction.*

zee@geomi.com

Janos L. Urai *is professor of structural geology and tectonics at RWTH Aachen University, Germany. He has an MSc in structural geology and crystallography from the University of Leiden, and a PhD in structural geology and geophysics from the University Utrecht. He has held Post-doctoral fellowships at the State University of New York, University of California at Davis and the Australian National University, and was Constantijn and Christiaan Huygens Fellow of NWO. After this he worked for seven years at the Shell Research Laboratories in Rijswijk, in structural geology, geomechanics and rock mechanics, on problems related to top and fault seal analysis, fault reactivation and wellbore stability. In 1995 he accepted the position currently held at RWTH Aachen University. Some of his current research interests are in the fields of top and fault seal evaluation, cementation of fractures and salt tectonics. He was Head of the Department of Geoscience. He is member of the editorial board of the Journal of Virtual Explorer. He has edited two books on structural geology and geomechanics and published a large number of papers in international journals. In 2002 he received the Andre Dumont Medal from Geologica Belgica.*

j.urai@ged.rwth-aachen.de

Pascal D. Richard *works as a Structural Geologist within the Carbonate Development Team at Shell International. He is based in Petroleum Devlopment Oman. Pascal has a PhD in Structural Geology on strike-slip tectonics, from the University of Rennes, France. Pascal joined Shell in 1991 and spent five years in KSEPL's Structural Geology Department on sandbox modeling of structural styles, fault growth and hydrocarbon systems. In 1996, he moved to Petroleum Development Oman (PDO) as the Structural Geology focal point and Seismic Interpreter with PDO's Exploration Department. In 1999 Pascal transferred to the Carbonate Development Team, where he is currently focusing on the analysis and modeling of fractured reservoirs.*

pascal.richard@pdo.co.om

For more information about the authors see, Geoscientist Directory at *www.gulfpetrolink.com*

Manuscript Received February 15, 2003

Revised April 10, 2003

Accepted April 15, 2003